Journal of the Korean Ceramic Society
Vol. 52, No. 6, pp. 514~520, 2015.

http://dx.doi.org/10.4191/kcers.2015.52.6.514

Microwave-Modified Sol-Gel Process for Microcystalline $KY(WO_4)_2$: Ho^{3+}/Yb^{3+} Phosphors and their Upconversion Photoluminescence Properties

Chang Sung Lim†

Department of Advanced Materials Science & Engineering, Hanseo University, Seosan 31962, Korea

(Received August 10, 2015; Revised October 5, November 12, 2015; Accepted November 16, 2015)

ABSTRACT

$KY_{1-x}(WO_4)_2$:Ho^{3+}/Yb^{3+} yellow phosphors with doping concentrations of Ho^{3+} and Yb^{3+} (x = Ho^{3+} + Yb^{3+}, Ho^{3+} = 0.05, 0.1, 0.2 and Yb^{3+} = 0.2, 0.45) were successfully prepared using the microwave-modified sol-gel method; their upconversion (UC) photoluminescence properties were investigated in detail. Well-crystallized particles, formed after heat-treatment at 900°C for 16 h, showed a fine and homogeneous morphology with particle sizes of 2-5 μm. Under excitation at 980 nm, the UC $KY_{0.7}(WO_4)_2$:$Ho_{0.1}Yb_{0.2}$ and $KY_{0.5}(WO_4)_2Ho_{0.05}Yb_{0.45}$ particles exhibited excellent yellow emissions based on a strong 545-nm emission band in the green region and a very strong 655-nm emission band in the red region. Pump power dependence and Commission Internationale de L'Eclairage chromaticity of the UC emission intensity were evaluated. The spectroscopic properties were examined comparatively using Raman spectroscopy.

Key words : Microwave sol-gel, Yellow phosphors, Upconversion, Raman spectroscopy

1. Introduction

The upconversion (UC) process, induced by trivalent lanthanide doped photoluminescence, converts long-wavelength excitation radiation in the infrared or near infrared regions to higher energy emission radiation in the ultraviolet to infrared regions. The UC photoluminescence particles have potential applications in various fields, including biomedical imaging, owing to their unique UC optical behaviors, which allow them to overcome many of the current limitations of traditional photoluminescence materials.[1-3] It is possible for the trivalent rare earth ions in the disordered tetragonal-phase to be partially substituted for by Ho^{3+} and Yb^{3+} ions; these ions are effectively doped into the crystal lattices of the tetragonal phase due to the similar radii of the trivalent rare earth ions in R^{3+}; this results in high red emitting efficiency and superior thermal and chemical stability. In these compounds, W^{6+} is coordinated by four O^{2-} ions at one tetrahedral site, which makes the resulting $[WO_4]^{2-}$ relatively stable. R^{3+} and M^{+} are randomly distributed over the same cationic sublattice; they are coordinated by eight O^{2-} molecules from the nearby four $[WO_4]^{2-}$ with a symmetry S_4 and without an inversion center.[4-6] The $[WO_4]^{2-}$ group has strong absorption in the near ultraviolet region, so that the energy transfer process from the $[WO_4]^{2-}$ group to the rare earth ions can easily occur, which can greatly enhance the external quantum efficiency of rare-earth ion doped materials.

Many lanthanides such as Er^{3+}, Tm^{3+}, and Ho^{3+} are used as luminescent centers because their abundant electronic energy levels are very convenient for realizing the conversion of near infrared light to visible light. Among the lanthanide ions, the Ho^{3+} ion as an activator is a promising UC luminescence center because of its unique luminescence in the visible range, when a sensitizer is used to enhance the UC luminescence efficiency. The Yb^{3+} ion is generally co-doped as a sensitizer owing to its strong absorption around 980 nm and can enhance the UC luminescence through energy transfer. Especially, due to the efficiency of the energy transfer from Yb^{3+} to Ho^{3+}, co-doped Yb^{3+} and Ho^{3+} ions can remarkably enhance the UC efficiency for the shift from infrared to visible light.[7-9]

Rare-earth doped double tungstates have been prepared using several processes including solid-state reactions,[10-12] the hydrothermal method,[13-18] the sol-gel method,[19] the solvothermal method,[20] the Pechini method,[21-23] and the combustion method.[24,25] Among the rare-earth doped double tungstates, only one, Er^{3+}/Yb^{3+} doped $KY(WO_4)_2$, was prepared by low-temperature liquid-phase epitaxy.[26] Compared with the usual methods, microwave synthesis has advantages of very short reaction time, small-size particles, narrow particle size distribution, and high purity of final polycrystalline samples. Microwave heating is delivered to the material surface by radiant and/or convection heating, which heat energy is transferred to the bulk of the material via conduction.[27] A microwave-modified sol-gel route is a cost-effective method that provides high homogeneity and is easy to scale up; it is emerging as a viable alternative approach for the quick synthesis of high-quality lumines-

†Corresponding author : Chang Sung Lim
E-mail : cslim@hanseo.ac.kr
Tel : +82-41-660-1445 Fax : +82-41-660-1445

cent materials. However, synthesis of $KY(WO_4)_2$:Ho^{3+}/Yb^{3+} phosphors via the microwave-modified sol-gel route has not yet been reported.

In this study, $KY_{1-x}(WO_4)_4$:Ho^{3+}/Yb^{3+} phosphors with the correct doping concentrations of Ho^{3+} and Yb^{3+} (x = Ho^{3+} + Yb^{3+}, Ho^{3+} = 0.05, 0.1, 0.2, and Yb^{3+} = 0.2, 0.45) phosphors were prepared by the cyclic microwave-assisted sol-gel method, followed by heat treatment. The synthesized particles were characterized by X-ray diffraction (XRD) and scanning electron microscopy (SEM). Pump power dependence and Commission Internationale de L'Eclairage (CIE) chromaticity of the UC emission intensity were evaluated in detail. The optical properties were examined comparatively using photoluminescence (PL) emission and Raman spectroscopy.

2. Experimental Procedure

Stoichiometric amounts of KNO_3 (99%, Sigma-Aldrich, USA), $Y(NO_3)_3{\cdot}6H_2O$ (99%, Sigma-Aldrich, USA), $(NH_4)_6W_{12}O_{39}{\cdot}xH_2O$ (99%, Alfa Aesar, USA), $Ho(NO_3)_3{\cdot}5H_2O$ (99.9%, Sigma-Aldrich, USA), $Yb(NO_3)_3{\cdot}5H_2O$ (99.9%, Sigma-Aldrich, USA), citric acid (99.5%, Daejung Chemicals, Korea), NH_4OH (A.R.), ethylene glycol (A.R.), and distilled water were used to prepare $KY(WO_4)_2$, $KY_{0.8}(WO_4)_2$:$Ho_{0.2}$, $KY_{0.7}(WO_4)_2$:$Ho_{0.1}Yb_{0.2}$, and $KY_{0.5}(WO_4)_2$:$Ho_{0.05}Yb_{0.45}$ compounds with the correct doping concentrations of Ho^{3+} and Yb^{3+} (Ho^{3+} = 0.05, 0.1, 0.2, and Yb^{3+}= 0.2, 0.45). To prepare $KY(WO_4)_2$, 0.4 mol% KNO_3 and 0.067 mol% $(NH_4)_6W_{12}O_{39}{\cdot}xH_2O$ were dissolved in 20 mL of ethylene glycol and 80 mL of 5 M NH_4OH under vigorous stirring and heating. Subsequently, 0.4 mol% $Y(NO_3)_3{\cdot}6H_2O$ and citric acid (with a molar ratio of citric acid to total metal ions of 2:1) were dissolved in 100 mL of distilled water under vigorous stirring and heating. Then, the solutions were mixed together under vigorously heated at 80 - 100°C. Finally, highly transparent solutions were obtained and adjusted to pH = 7 - 8 by the addition of NH_4OH or citric acid. In order to prepare $KY_{0.8}(WO_4)_2$:$Ho_{0.2}$, the mixture of 0.32 mol% $Y(NO_3)_3{\cdot}6H_2O$ with 0.08 mol% $Ho(NO_3)_3{\cdot}5H_2O$ was used for the creation of the rare earth solution. In order to prepare $KY_{0.7}(WO_4)_2$:$Ho_{0.1}Yb_{0.2}$, the mixture of 0.28 mol% $Y(NO_3)_3{\cdot}6H_2O$ with 0.04 mol% $Ho(NO_3)_3{\cdot}5H_2O$ and 0.08 mol% $Yb(NO_3)_3{\cdot}5H_2O$ was used for the creation of the rare earth solution. In order to prepare $KY_{0.5}(WO_4)_2$:$Ho_{0.05}Yb_{0.45}$, the solution containing the rare earth materials was generated using 0.2 mol% $Y(NO_3)_3{\cdot}6H_2O$ with 0.02 mol% $Ho(NO_3)_3{\cdot}5H_2O$ and 0.18 mol% $Yb(NO_3)_3{\cdot}5H_2O$.

The transparent solutions were placed in a microwave oven operating at a frequency of 2.45 GHz with a maximum output-power of 1250 W for 30 min. The working cycle of the microwave reaction was controlled very precisely using a regime of 40 s on and 20 s off for 15 min, followed by further treatment of 30 s on and 30 s off for 15 min. The ethylene glycol was evaporated slowly at its boiling point. Ethylene glycol is a polar solvent at its boiling point of 197°C; this solvent is a good candidate for the microwave process. If ethylene glycol is used as the solvent, the reactions proceed at the boiling point temperature. When microwave radiation is supplied to the ethylene-glycol-based solution, the components dissolved in the ethylene glycol can couple. The charged particles vibrate interdependently in the electric field when a large amount of microwave radiation is supplied to the ethylene glycol. The samples were treated with ultrasonic radiation for 10 min to produce a light yellow transparent sol. After this, the light yellow transparent sols were dried at 120°C in a dry oven to obtain black dried gels. The black dried gels were ground and heat-treated at 900°C for 16 h at 100°C intervals between 600-900°C. Finally, white particles were obtained for $KY(WO_4)_2$ and pink particles were obtained for the doped compositions.

The phase composition of the synthesized particles was identified using XRD (D/MAX 2200, Rigaku, Japan). The microstructure and surface morphology of the $KY(WO_4)_2$, $KY_{0.8}(WO_4)_2$:$Ho_{0.2}$, $KY_{0.7}(WO_4)_2$:$Ho_{0.1}Yb_{0.2}$, and $KY_{0.5}(WO_4)_2$:$Ho_{0.05}Yb_{0.45}$ particles were observed using SEM/EDS (JSM-5600, JEOL, Japan). The PL spectra were recorded using a spectrophotometer (Perkin Elmer LS55, UK) at room temperature. Pump power dependence of the UC emission intensity was measured at levels of working power from 20 to 110 mW. Raman spectra measurements were performed using a LabRam Aramis (Horiba Jobin-Yvon, France) with a spectral resolution of 2 cm^{-1}. The 514.5-nm line of an Ar ion laser was used as an excitation source; to avoid sample decomposition, the samples were exposed to a power level that was maintained at 0.5 mW.

3. Results and Discussion

Figure 1 shows the X-ray diffraction patterns of (a) the JCPDS 45-0472 pattern of $KY(WO_4)_2$, the synthesized (b) $KY(WO_4)_2$, (c) $KY_{0.8}(WO_4)_2$:$Ho_{0.2}$, (d) $KY_{0.7}(WO_4)_2$:$Ho_{0.1}Yb_{0.2}$, and (e) $KY_{0.5}(WO_4)_2$:$Ho_{0.05}Yb_{0.45}$ particles. It was possible to

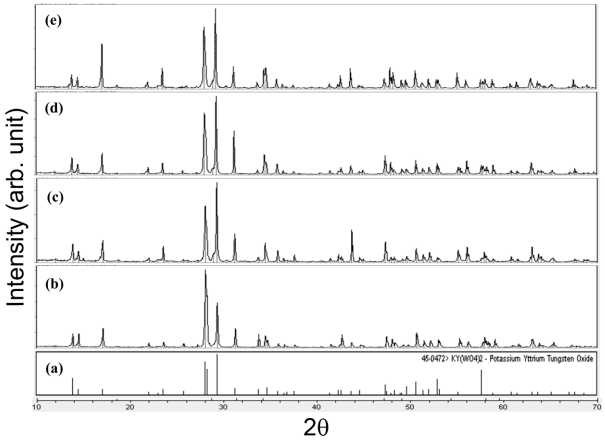

Fig. 1. X-ray diffraction patterns of the (a) JCPDS 45-0472 pattern of $KY(WO_4)_2$, the synthesized (b) $KY(WO_4)_2$, (c) $KY_{0.8}(WO_4)_2$:$Ho_{0.2}$, (d) $KY_{0.7}(WO_4)_2$:$Ho_{0.1}Yb_{0.2}$, and (e) $KY_{0.5}(WO_4)_2$:$Ho_{0.05}Yb_{0.45}$ particles.

assign almost all of the XRD peaks to the monoclinic-phase $KY(WO_4)_2$; this is in good agreement with the crystallographic data of $KY(WO_4)_2$ (JCPDS 45-0472). The XRD shows impurity peaks in the 2 theta ranges of 15-20 and 24-28 degrees. The secondary phases are assumed to be one of the WO_{4-x} groups ($W_{18}O_{49}$, W_5O_{14}, $W_{24}O_{68}$). However, it is very difficult to identify the secondary phases because very weak peaks are observed, and the WO_{4-x} has very similar and complicated reflexes. The $KY(WO_4)_2$ structure is of monoclinic (space group *C*2/c) centrosymmetric scheelite-type with unit-cell parameters of a=10.64 Å, b=10.35 Å, c= 7.54 Å, and β = 130.5°.[28] In the doped crystals, the unit cell shrinkage results from the substitution of Y^{3+} ions by Ho^{3+} and Yb^{3+} ions. It is assumed that the radiuses of Ho^{3+} (R=1.015 Å) and Yb^{3+} (R = 0.985 Å) are smaller than that of Y^{3+} (R=1.019 Å) when the coordination number is CN = 8.[29] Consequently, it should be emphasized that the Ho^{3+} and Yb^{3+} ions can be effectively doped in the $KY_{1-x}(WO_4)_2$ lattice by partial substitution of Y^{3+} sites. It leads to unit cell shrinkage due to the similar radii of Y^{3+}, and by Ho^{3+} and Yb^{3+} while maintaining the monoclinic structure of the $KY_{1-x}(WO_4)_2$. This means that the obtained samples possess a monoclinic phase after partial substitution of Y^{3+} by Ho^{3+} and Yb^{3+} ions; it also means that the ions are effectively doped into the crystal lattices of the $KY(WO_4)_2$ phase due to the similar radii of Y^{3+} and by Ho^{3+} and Yb^{3+}. Post heat-treatment plays an important role in a well-defined crystallized morphology. To achieve a well-defined crystalline morphology, $KY(WO_4)_2$, $KY_{0.8}(WO_4)_2$:$Ho_{0.2}$, $KY_{0.7}(WO_4)_2$:$Ho_{0.1}Yb_{0.2}$, and $KY_{0.5}(WO_4)_2$:$Ho_{0.05}Yb_{0.45}$ phases need to be heat treated at 900°C for 16 h. It is assumed that the doping amount of Ho^{3+}/Yb^{3+} has a great effect on the crystalline cell volume of $KY(WO_4)_2$ because of the different ionic sizes.

Figure 2 provides an SEM image of the synthesized $KY_{0.5}(WO_4)_2$:$Ho_{0.05}Yb_{0.45}$ particles. The as-synthesized sample is well crystallized, with a fine and homogeneous morphology and particle size of 2-5 μm. It should be noted that the structure has a monoclinic phase after partial substitution of Y^{3+} by Ho^{3+} and Yb^{3+} ions; the ions are effectively doped into the crystal lattices of the $KY(WO_4)_2$ phase. The microwave sol-gel process of the double tungstates provides the energy to synthesize the bulk of the material uniformly, so that fine particles with controlled morphology can be fabricated in a short time period. This method is a cost-effective way to fabricate highly homogeneous products and is easy to scale-up; it is a viable alternative for the rapid synthesis of UC particles.

Figure 3 shows the UC photoluminescence emission spectra of the as-prepared (a) $KY(WO_4)_2$, (b) $KY_{0.8}(WO_4)_2$:$Ho_{0.2}$, (c) $KY_{0.7}(WO_4)_2$:$Ho_{0.1}Yb_{0.2}$, and (d) $KY_{0.5}(WO_4)_2$: $Ho_{0.05}Yb_{0.45}$ particles excited under 980 nm emission at room temperature. The UC (c) $KY_{0.7}(WO_4)_2$:$Ho_{0.1}Yb_{0.2}$ and (d) $KY_{0.5}(WO_4)_2Ho_{0.05}Yb_{0.45}$ particles exhibited yellow emissions based on a strong 545-nm emission band in the green region and a very strong 655-nm emission band in the red region. The UC intensities of (a) $KY(WO_4)_2$ and (b) $KY_{0.8}(WO_4)_2$:$Ho_{0.2}$ particles were not

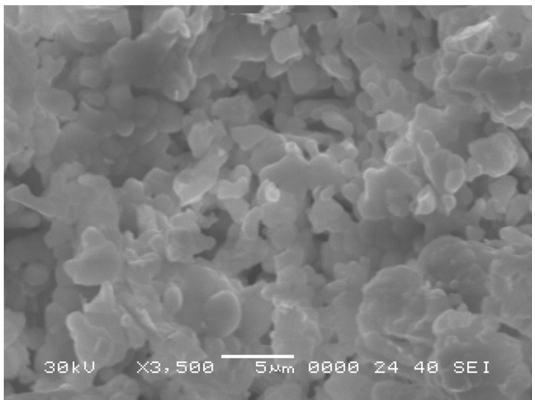

Fig. 2. Scanning electron microscopy image of the synthesized $KY_{0.5}(WO_4)_2$:$Ho_{0.05}Yb_{0.45}$ particles.

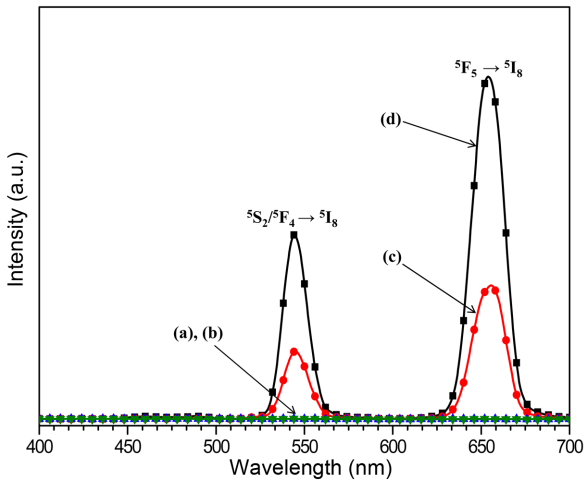

Fig. 3. Upconversion photoluminescence emission spectra of (a) $KY(WO_4)_2$, (b) $KY_{0.8}(WO_4)_2$:$Ho_{0.2}$, (c) $KY_{0.7}(WO_4)_2$:$Ho_{0.1}Yb_{0.2}$, and (d) $KY_{0.5}(WO_4)_2$:$Ho_{0.05}Yb_{0.45}$ particles excited under 980 nm emission at room temperature.

detected. The UC intensity of (d) $KY_{0.5}(WO_4)_2$:$Ho_{0.05}Yb_{0.45}$ particles is much higher than that of (c) $KY_{0.7}(WO_4)_2$:$Ho_{0.1}Yb_{0.2}$ particles. The strong 550-nm emission band in the green region corresponds to the $^5S_2/^5F_4 \rightarrow {}^5I_8$ transition, while the very strong 655-nm emission band in the red region corresponds to the $^5F_5 \rightarrow {}^5I_8$ which is a transfer to the activator, where radiation can be emitted. The Ho^{3+} ion activator is the luminescence center of these UC particles, and the sensitizer Yb^{3+} effectively enhances the UC luminescence intensity because of the efficient energy transfer from Yb^{3+} to Ho^{3+}. The higher intensity of $KY_{0.5}(WO_4)_2$:$Ho_{0.05}Yb_{0.45}$ caused the ratio of Yb^{3+}:Ho^{3+} to be 9:1, whereas the higher content of the Yb^{3+} ion, used as a sensitizer owing to its strong absorption at around 980 nm, can remarkably enhance the UC luminescence through energy transfer.

The logarithmic scale dependence of the UC emission intensities at 545 and 655 nm on the working pump power over the range of 20 to 110 mW in the $KY_{0.5}(WO_4)_2$:$Ho_{0.05}Yb_{0.45}$ sample is shown in Fig. 4. In the UC process, the UC emission intensity is proportional to the slope value *n* of

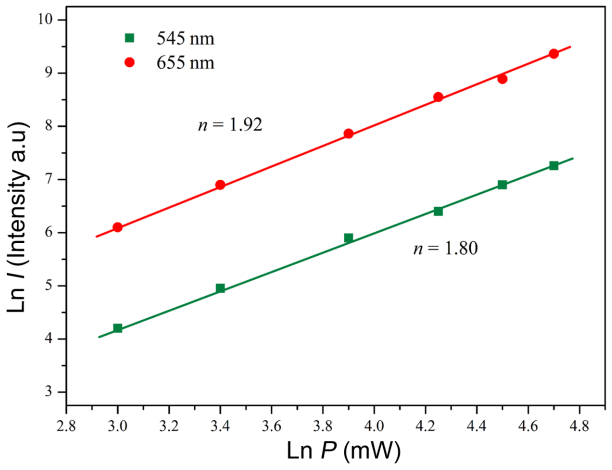

Fig. 4. Logarithmic scale of pump power dependence of the upconversion emission intensity on the working current from 20 to 110 mW at 545 and 655 nm in the $KY_{1-x}(WO_4)_2$:Ho^{3+}/Yb^{3+} system.

the irradiation pumping power, where n is the number of pumped photons required to produce UC emission[30,31]:

$$I \propto P^n$$
$$\mathrm{Ln}I \propto n\mathrm{Ln}P$$

where the value n is the number of the pumped photons required to excite the upper emitting state, I is the UC luminescent intensity, and P is the laser pumping power. The calculated slope value n , shown in Fig. 4, indicate a slope n = 1.80 for green emission at 545 nm; this value is 1.92 for red emission at 655 nm. These results show that the UC mechanism of the green and red emissions can be explained by a two-photon UC process in Ho^{+3}/Yb^{3+} co-doped phosphors.[14-18]

Based on the results of the analysis of pump power dependence, the known schematic energy level diagrams of Ho^{3+} (activator) and Yb^{3+} (sensitizer) ions in the as-prepared $KY_{1-x}(WO_4)_2$:Yb_y/Ho_z samples, and the UC mechanisms accounting for the green and red emissions during 980 nm laser excitation, are shown in Fig. 5. The UC emissions are generated by a two photon process of excited state absorption (ESA) and energy transfer (ET). Initially, the Yb^{3+} ion sensitizer is excited from the $^2F_{7/2}$ level to the $^2F_{5/2}$ level under excitation resulting from 980 nm emission; the Yb^{3+} ion sensitizer transfers its energy to the Ho^{3+} ions. Then, the Ho^{3+} ions are populated from the $^5I_8$ ground state to the $^5I_6$ excited state. This is a phonon-assisted energy transfer process because of the energy mismatch between the $^2F_{5/2}$ level of Yb^{3+} and the $^5I_6$ level of Ho^{3+}. Second, the Ho^{3+} in the $^5I_6$ level is excited to the $^5S_2$ or $^5F_4$ level by the next energy transfer from Yb^{3+}. In addition, the $^5S_2$ /$^5F_4$ level of Ho^{3+} can be populated through the excited state absorption. Finally, the green emission at around 545 nm, corresponding to the $^5S_2$/$^5F_4 \rightarrow {}^5I_8$ transition, takes place. For the red emission, the population of the $^5F_5$ level is generated by two different

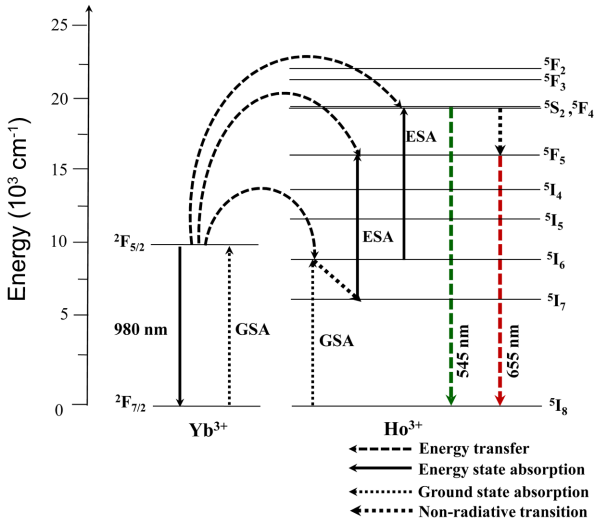

Fig. 5. Schematic energy level diagrams of Ho^{3+} ions (activator) and Yb^{3+} ions (sensitizer) in the as-prepared $KY_{1-x}(WO_4)_2$:Ho^{3+}/Yb^{3+} system and the upconversion mechanisms accounting for the green and red emissions under 980-nm laser excitation.

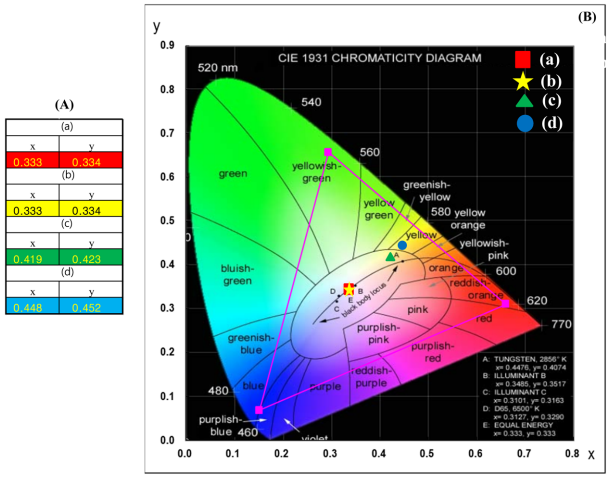

Fig. 6. (A) Calculated chromaticity coordinate (x, y) values and (B) CIE chromaticity diagram for (a) $KY(WO_4)_2$, (b) $KY_{0.8}(WO_4)_2$:$Ho_{0.2}$, (c) $KY_{0.7}(WO_4)_2$:$Ho_{0.1}Yb_{0.2}$, and (d) $KY_{0.5}(WO_4)_2$:$Ho_{0.05}Yb_{0.45}$ particles.

channels. One channel is the results of Ho^{3+} in the $^5S_2/^5F_4$ level state relaxing non-radiatively to the $^5F_5$ level. The other channel is closely related to the $^5I_7$ level populated by non-radiative relaxation from the $^5I_6$ excited state. The Ho^{3+} in the $^5I_7$ level is excited to the $^5F_5$ level by the energy transfer from Yb^{3+} and relaxes to the $^5F_5$ level. Therefore, the red emission around 655 nm corresponds to the $^5F_5 \rightarrow {}^5I_8$ transition.[31-33]

Figure 6 shows (A) calculated chromaticity coordinate (x, y) values and (B) CIE chromaticity diagram for (a) $KY(WO_4)_2$, (b) $KY_{0.8}(WO_4)_2$:$Ho_{0.2}$, (c) $KY_{0.7}(WO_4)_2$:$Ho_{0.1}Yb_{0.2}$, and (d) $KY_{0.5}(WO_4)_2$:$Ho_{0.05}Yb_{0.45}$ particles. The triangle shown in Fig. 6(B) indicates the standard color coordinates for blue, green, and

red. The insets in Fig. 6(B) show the chromaticity points for the samples (a), (b), (c), and (d). When the concentration ratios of Ho^{3+}/Yb^{3+} are modulated, the chromaticity coordinate values (x, y) change. As can be seen in Fig. 6, the calculated chromaticity coordinates x = 0.419 and y = 0.423 for (c) $KY_{0.7}(WO_4)_2$:$Ho_{0.1}Yb_{0.2}$, and x = 0.448 and y = 0.452 for (d) $KY_{0.5}(WO_4)_2$:$Ho_{0.05}Yb_{0.45}$ correspond to yellow emissions and the standard equal energy point in the CIE diagram. This result indicates the achievement of attractive yellow UC emissions for use in potentially active components in new optoelectronic devices and luminescent devices.

Figure 7 shows the Raman spectra of the synthesized (a) $KY(WO_4)_2$, (b) $KY_{0.8}(WO_4)_2$:$Ho_{0.2}$, (c) $KY_{0.7}(WO_4)_2$:$Ho_{0.1}Yb_{0.2}$, and (d) $KY_{0.5}(WO_4)_2$:$Ho_{0.05}Yb_{0.45}$ particles excited by the 514.5-nm line of an Ar ion laser at 0.5 mW. The internal modes for the (a) $KY(WO_4)_2$ particles were detected at 180, 224, 320, 350, 378, 442, 530, 686, 765, 810, and 905 cm^{-1}. The well-resolved sharp peaks for the $KY(WO_4)_2$ particles indicate the high crystallinity state of the synthesized particles. The internal vibration frequencies are dependent on the lattice parameters and the strength of the partially covalent bond between the cations and the molecular ionic groups of WO_x. For the $KY(WO_4)_2$ crystal, shown in Fig. 7(a), the highest wavenumber band at 905 cm^{-1} corresponds to stretching vibrations of the W-O bonds. The stretching vibrations of WO_4 are observed in the 765 and 810 cm^{-1} regions. For these stretching vibrations, strong mixing occurs between the W-O bonds and the WO_4. The band at 530 cm^{-1} could be assumed to originate from vibrations of the longer W-O bonds, which are employed in the formation of the W-W bridge. The corresponding bending vibrations are seen at 350 - 442 cm^{-1}. The translational vibration motion of the K^+ ions is observed at 224 cm^{-1}, whereas the Y^{3+} translations are located at levels lower than 180 cm^{-1}.

The Raman spectra of the doped particles indicate strong disordered peaks at higher frequencies of 686, 732, 762, 906, and 932 cm^{-1} and weak peaks at lower frequencies near 320 cm^{-1}. Basically, the spectra of the doped samples are similar to the Raman spectra of the undoped sample, which contributes to maintaining the monoclinic structure of the undoped $KY(WO_4)_2$. The strong disordered peaks of the doped samples can be attributed to the formation of highly modulated structures of the WO_{4-x} group induced by the strong mixing of stretching vibrations between the W-O bonds and the WO_4. It should be noted that the unit cell shrinkage accompanying the highly modulated structure with the WO_{4-x} group in the $KY_{1-x}(WO_4)_2$ incorporated by $Ho^{3+}$and Yb^{3+} ions strongly affects the upconversion intensities according to the doping concentrations of Ho^{3+} and Yb^{3+}.[31] It should be emphasized that the highly modulated structure has strong absorption in the near ultraviolet region, so that energy transfer processes from the WO_{4-x} group to rare earth ions can easily occur; these processes can greatly enhance the external quantum efficiency of the rare earth ion doped materials. These results lead to high emitting efficiency and

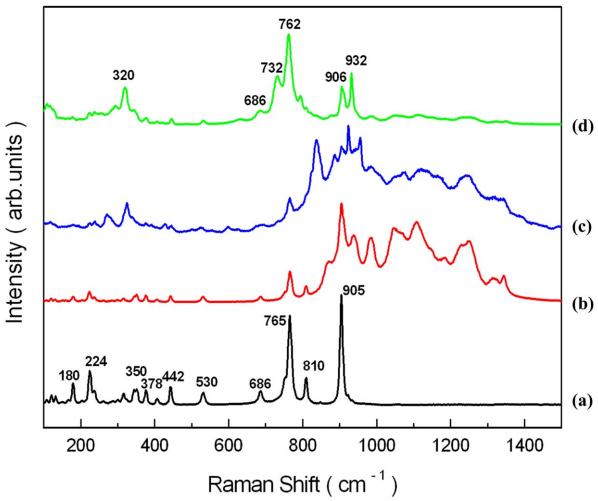

Fig. 7. Raman spectra of the synthesized (a) $KY(WO_4)_2$, (b) $KY_{0.8}(WO_4)_2$:$Ho_{0.2}$, (c) $KY_{0.7}(WO_4)_2$:$Ho_{0.1}Yb_{0.2}$, and (d) $KY_{0.5}(WO_4)_2$:$Ho_{0.05}Yb_{0.45}$ particles excited by the 514.5-nm line of an Ar ion laser at 0.5 mW.

superior thermal and chemical stability; these materials, which can overcome the current limitations of traditional photoluminescence materials, can be considered potentially active components in new optoelectronic devices and in luminescent imaging.

4. Conclusions

$KY_{1-x}(WO_4)_2$:Ho^{3+}/Yb^{3+} yellow phosphors with correct doping concentrations of Ho^{3+} and Yb^{3+} (x = Ho^{3+} + Yb^{3+}, Ho^{3+} = 0.05, 0.1, 0.2, and Yb^{3+} = 0.2, 0.45) were successfully prepared using the microwave-modified sol-gel method. Well-crystallized particles, formed after heat-treatment at 900°C for 16 h, showed a fine and homogeneous morphology with particle sizes of 2-5 μm. Under excitation at 980 nm, the UC $KY_{0.7}(WO_4)_2$:$Ho_{0.1}Yb_{0.2}$ and $KY_{0.5}(WO_4)_2$:$Ho_{0.05}Yb_{0.45}$ particles exhibited yellow emissions based on a strong 545-nm emission band in the green region and a very strong 655-nm emission band in the red region; these bands were assigned to the $^5S_2/^5F_4 \rightarrow {}^5I_8$ and $^5F_5 \rightarrow {}^5I_8$ transitions, respectively. The higher intensity emission of $KY_{0.5}(WO_4)_2$:$Ho_{0.05}Yb_{0.45}$ caused the ratio of Yb^{3+}:Ho^{3+} to be 9:1, whereas the higher content of the Yb^{3+} ion, used as a sensitizer owing to its strong absorption at around 980 nm, was found to remarkably enhance the UC luminescence through energy transfer. The strong disordered peaks of the doped samples were attributed to the formation of highly modulated structures of the WO_{4-x} group, induced by the strong mixing of stretching vibrations between the W-O bonds and the WO_4. These results led to high emitting efficiency and the involved materials can be considered potentially active components in new optoelectronic devices and in the field of luminescent imaging.

Acknowledgments

This study was supported by the Research Program through the Campus Research Foundation funded by Hanseo University in 2015 (151Egong06).

REFERENCES

1. M. V. DaCosta, S. Doughan, and U. J. Krull, "Lanthanide Upconversion Nanoparticles and Application in Bioassays and Bioimaging: A Review," *Analyca Chimica Acta*, **832** [3] 1-33 (2014).
2. M. Lin, Y. Zho, S. Wang, M. Liu, Z. Duan, Y. Chen, F. Li, F. Xu, and T. Lu, "Recent Advances in Synthesis and Surface Modification of Lanthanide-doped Upconversion Nanoparticles for Biomedical Napplications," *Biotechnol. Adv.*, **30** [6] 1551-61 (2012).
3. M. Wang, G. Abbineni, A. Clevenger, C. Mao, and S. Xu, "Upconversion Nanoparticles: Synthesis, Surface Modification and Biological Applications," *Nanomed.: Nanotech. Biol. Med.*, **7** [6] 710-29 (2011).
4. L. Li, W. Zi, H. Yu, S. Gan, G. Ji, H. Zou, and X. Xu, "Synthesis and Luminescence Properties of High Brightness $MLa(WO_4)_2$:Eu^{3+} (M=Li, Na, K) and $NaRE(WO_4)_2$:Eu^{3+} (RE=Gd, Y, Lu) Red Phosphors," *J. Lumin.,* **143** [1] 14-20 (2013).
5. C. Ming, F. Song, and L. Yan, "Spectroscopic Study and Green Upconversion of Pr^{3+}/Yb^{3+}-Codoped $NaY(WO_4)_2$ Crystal, " *Opt. Commun.*, **286** [8] 217-20 (2013).
6. N. Xue, X. Fan, Z. Wang, and M. Wang, "Synthesis Process and the Luminescence Properties of Rare Earth Doped $NaLa(WO_4)_2$ Nanoparticles," *J. Phys. Chem. Sol.*, **69** [8] 1891 (2008).
7. Z. Shan, D. Chen, Y. Yu, P. Huang, F. Weng, H. Lin, and Y. Wang, "Upconversion Luminescence of Ho^{3+} Sensitized by Yb^{3+} in Transparent Glass Ceramic Embedding $BaYF_5$ Nanocrystals," *Mater. Res. Bull.*, **45** [8] 1017-20 (2010).
8. W. Liu, J. Sun, X. Li, J. Zhang, Y. Tian, S. Fu, H. Zhong, T. Liu, L. Cheng, H. Xia, B. Dong, R. Hua, X. Zhang, and B. Chen, "Laser Induced Thermal Effect on Upconversion Luminescence and Temperature-Dependent Upconversion Mechanism in Ho^{3+}/Yb^{3+}-Codoped $Gd_2(WO_4)_3$ Phosphor," *Opt. Mater.*, **35** [7] 1487-92 (2013).
9. W. Xu, H. Zhao, Y. Li, L. Zheng, Z. Zhang, and W. Cao, "Optical Temperature Sensing through the Upconversion Luminescence from Ho^3+/Yb^{3+} Codoped $CaWO_4$," *Sensors and Act. B:Chem.*, **188** [11] 1096-100 (2013).
10. H. Du, Y. Lan, Z. Zhiguo, and J. Sun, "Upconversion Luminescence of $Yb^{3+}/Ho^{3+}/Er^{3+}/Tm^{3+}$ Co-doped $KGd(WO_4)_2$ Powders," *J. Rare Earths*, **28** [5] 697-700 (2010).
11. X. Liu, W. Xiang, F. Chen, W. Zhang, and Z. Hu, "Synthesis and Photoluminescence of Tb^{3+} Activated $NaY(WO_4)_2$ Phosphors," *Mater. Res. Bull.*, **47** [11] 3417-21 (2012).
12. X. Liu, W. Xiang, F. Chen, Z. Hu, and W. Zhang, "Synthesis and Photoluminescence Characteristics of Dy^{3+} Doped $NaY(WO_4)_2$ Phosphors," *Mater. Res. Bull.*, **48** [2] 281-85 (2013).
13. N. Xue, X. Fan, Z. Wang, and M. Wang, "Synthesis Process and Luminescence Properties of Ln^{3+} Doped $NaY(WO_4)_2$ Nanoparticles," *Mater. Lett.*, **61** [7] 1576-79 (2007).
14. X. Yu, Y. Qin, M. Gao, L. Duan, Z. Jiang, L. Gou, P. Zhao, and Z. Li, "Hydrothermal Synthesis and Upconversion Luminescence of $NaGd(WO_4)_2$ Co-doped with Ho^{3+} and Yb^{3+}," *J. Lumin.*, **153** [9] 1-4 (2014).
15. S. Huang, D. Wang, Y. Wang, L. Wang, X. Zhang, and P. Yang, "Self-Assembled Three-Dimensional $NaY(WO_4)_2$:Ln^{3+} Architectures: Hydothermal Synthesis, Growth Mechanism and Luminescence Properties," *J. Alloys Compd.*, **529** [7] 140-47 (2012).
16. J. Liao, B. Qiu, and H. Lai, "Synthesis and Luminesecnce Properties of Tb^{3+}:$NaGd(WO_4)_2$ Novel Green Phosphors," *J. Lumin.*, **129** [7] 668-71 (2009).
17. X. Yu, M. Gao, J. Li, L. Duan, N. Cao, Z. Jiang, A. Hao, P. Zhao, and J. Fan, "Near Infrared to Visible Upconversion Emission in Er^{3+}/Yb^{3+} Co-doped $NaGd(WO_4)_2$ Nanoparticles Obtained by Hydrothermal Method," *J. Lumin.*, **154** [10] 111-15 (2014).
18. J. Gu, Y. Zhu, H. Li, S. Xiong, X. Zhang, X. Wang, X. Liu, and Y. Qian, "Morphology Controllable Synthesis and Luminescence Properties of $NaLa(WO_4)_2$:Eu Microcrystals," *Solid State Sci.*, **12** [7] 1192-98 (2010).
19. D. Thangaraju, A. Durairajan, D. Balaji, and S. M. Babu, "Synthesis and Characterization of Monoclinic $KGd(WO_4)_2$ Particles for Non-Cubic Transparent Ceramics," *Opt. Mater.*, **35** [4] 753-56 (2013).
20. J. Gu, Y. Zhu, H. Li, X. Zhang, and Y. Qian, "Uniform Ln^{3+}(Eu^{3+}, Tb^{3+}) Doped $NaLa(WO_4)_2$ Nanocrystals: Synthesis, Characterization, and Optical Properties," *J. Solid State Chem.*, **183** [3] 497-503 (2010).
21. P. Pazik, A. Zych, and W. Strek, "Luminescence Properties of Eu^{3+}:$KGd(WO_4)_2$ Nnocrystallites," *Mater. Chem. Phys.*, **115** [2-3] 536-40 (2009).
22. A. Durairajan, D. Thangaraju, D. Balaji, and S. M. Babu, "Sol-Gel Synthesis and Characterizations of Crystalline $NaGd(WO_4)_2$ Powder for Anisotropic Transparent Ceramic Laser Application," *Opt. Mater.*, **35** [4] 740-43 (2013).
23. L. Macalik, P. E. Tomaszewski, R. Lisiecki, and J. Hanuza, "The Crystal Structure, Vibrational and Luminescence Properties of the Nanocrystlline $KEu(WO_4)_2$ and $KGd(WO_4)_2$: Eu^{3+} Obtained by the Pechini Method," *J. Solid State Chem.*, **181** [10] 2591-2600 (2008).
24. Z. Lu and T. Wanjun, "Synthesis and Luminescence Properties of Eu^{3+}-Activated $NaLa(MoO_4)(WO_4)$ Phosphor," *Ceram. Int.*, **38** [1] 837-40 (2012).
25. X. Qian, X. Pu, D. Zhang, L. Li, M. Li, and S. Wu, "Combustion Synthesis and Luminescence Properties of $NaY_{1-x}Eu_x(WO_4)_2$ Phosphors," *J. Lumin.*, **131** [8] 1692-95 (2011).
26. S. Garcia-revilla, R. Valiente, Y. E. Romanyuk, and M. Pollnau, "Temporal Dynamics of Upconversion Luminescence in Er^{3+}, Yb^{3+} Co-doped Crystalline $KY(WO_4)_2$ Thin Films," *J. Lumin.*, **128** [5-6] 934-36 (2008).
27. C. S. Lim, "Cyclic MAM Synthesis and Upconversion Photoluminescence Properties of $CaMoO_4$:Er^{3+}/Yb^{3+} Particles," *Mater. Res. Bull.*, **47** [12] 4220-25 (2012).
28. V. L. Bekenev, O. Y. Khyzhun, and V. V. Atuchin, "Electronic Structure of Monoclinic α-$KY(WO_4)_2$ Tungstates as Determined from First-Principles FP-LAPW Calculations and X-ray Spectroscopy Studies," *J. Alloys Compd.,* **485** [1]

51-8 (2009).
29. R. D. Shanan, "Revised Effective Ionic Radii and Systematic Studies of Interatomic Distances in Halides and Chalcogenides," *Acta Cryst. A,* **32** [3] 751-67 (1976).
30. H. Guo, N. Dong, M. Yin, W. Zhang, L. Lou, and S. Xia, "Visible Upconversion in Rare Earth-doped Gd_2O_3 Nanocrystals," *J. Phys. Chem. B,* **108** [10] 19205-9 (2004).
31. C. S. Lim, A. Aleksandrovsky, M. Molokeev, A. Oreshonkov, and V. Atuchin, "The Modulated Structure and Frequency Upconversion Properties of $CaLa_2(MoO_4)_4$:Ho^{3+}/Yb^{3+} Phosphors Prepared by Microwave Synthesis," *Phys. Chem. Chem. Phys.*, **17** [9] 19278-87 (2015)
32. Y. Xu, Y. Wang, L. Shi, L. Xing, and X. Tan, "Bright White Upconversion Luminescence in Ho^{3+}/Yb^{3+}/Tm^{3+} Triple Doped $CaWO_4$ Polycrystals," *Opt. Laser Tech.*, **54** [1] 50-2 (2013).
33. X. Li, Q. Nie, S. Dai, T. Xu, L. Lu, and X. Zhang, "Energy Transfer and Frequency Upconversion in Ho^{3+}/Yb^{3+} Co-doped Bismuth-Germanate Glasses," *J. Alloys Compd.*, **454** [1-2] 510-14 (2008).